'Breathing-Crystals'

The Origin of Electrochemical Activity of Mesoporous Li-MnO2

Thi X.T. Sayle,[1,2] Kenneth Kgatwane,[2] Phuti E. Ngoepe[2] and Dean C. Sayle[1,*]

[1] School of Physical Sciences, University of Kent, Canterbury, CT2 7NZ, UK

*d.c.sayle@kent.ac.uk

[2] Materials Modelling Centre, University of Limpopo, Private Bag x1106, Sovenga, 0727, South Africa.

ABSTRACT: MD simulations reveal that mesoporous Li-MnO2 is electrochemically active because the stress, associated with charge cycling, does not influence the structure or dimensions of the (unlithiated) 1x1 tunnels in which the lithium ions intercalate and reside. Conversely, the parent bulk material suffers structural collapse and blockage of the 1x1 tunnels under stress. Akin to Le Chatalier's principle, we show that a mesoporous material can mitigate the effect of stress by expanding or contracting elastically into the pores of the mesoporous material; we simulate this 'breathing-crystal' phenomenon using MD simulation and show the mechanism of Li deintercallation from the mesoporous host lattice.

Supporting Information

Uniaxial Stress

The structural response of mesoporous MnO_2 to uniaxial stress is shown in fig. S1. Our simulations reveal that unlithiated and lithiated ($Li_{0.03}MnO_2$, $Li_{0.24}MnO_2$, $Li_{0.72}MnO_2$) mesoporous MnO_2 respond elastically under uniaxial compression, up to strains of about 4-7%, fig S1(c-f), with corresponding yield stresses of about 5-7 GPa. Tensile yield strains and stresses are slightly lower at about 4-6% (yield strain) and 3-5GPa (yield stress). The simulations reveal that Li intercalation weakens the system; yield stresses (compression and tension) are reduced as lithium is gradually intercalated into the lattice.

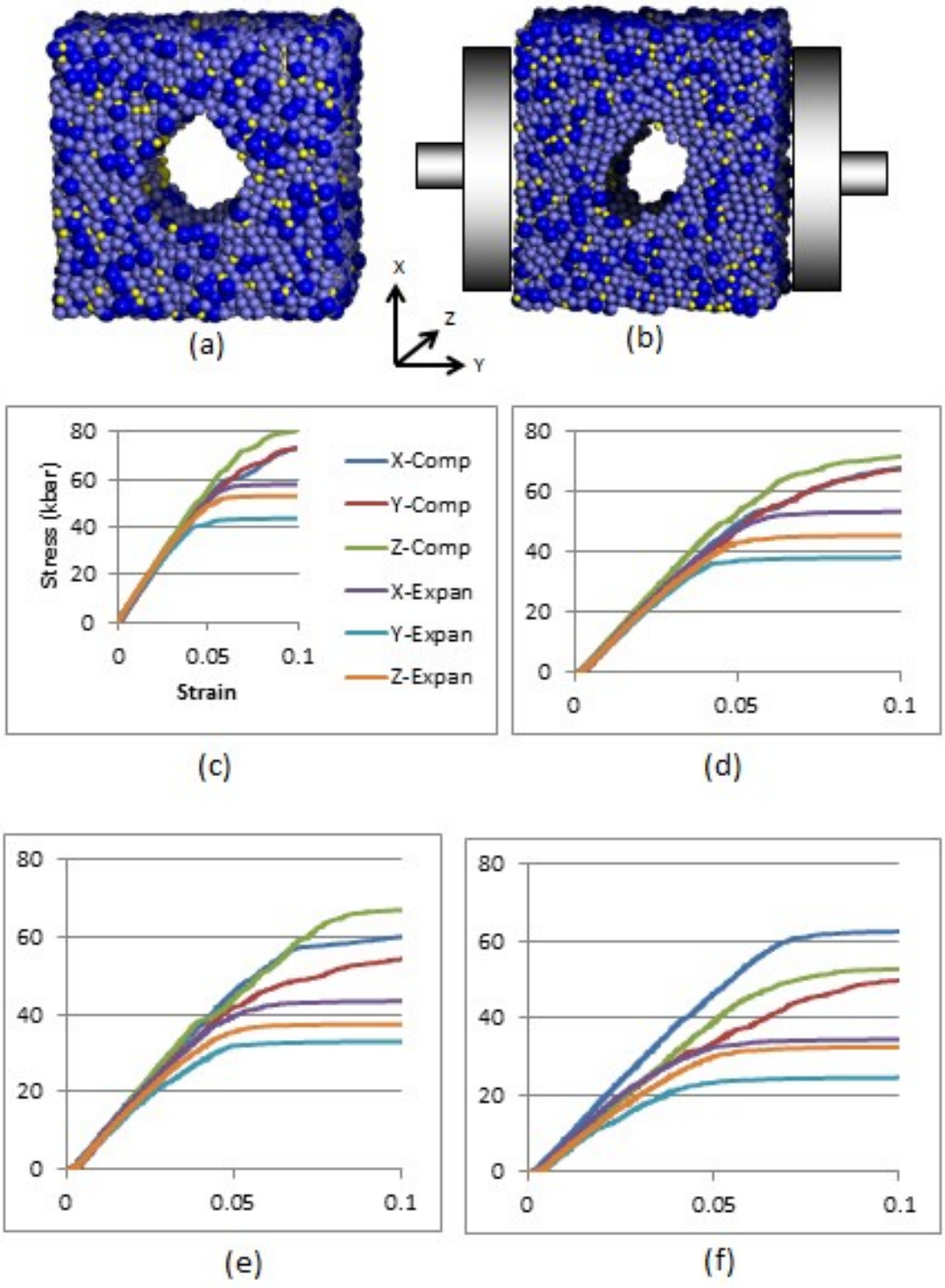

Figure S1 *Uniaxial compression (Comp) and tension (Expan) of mesoporous MnO_2. Structure of mesoporous $Li_{0.24}MnO_2$ (a) before and (b) after 50kbar uniaxial stress. Stress-strain curves for mesoporous β-MnO_2: (c) unlithiated, (d) $Li_{0.03}MnO_2$, (e) $Li_{0.24}MnO_2$, (f) $Li_{0.72}MnO_2$.*

Radial Distribution Functions (RDF)

Calculated RDF provide information as to the strain state of the mesoporous and bulk MnO_2. The Mn-Mn RDF, calculated for the bulk and mesoporous β-MnO_2 as a function of strain, are shown in fig. S2(a), bulk, and S2(b), mesoporous. The RDFs were used to gauge the structural integrity of the system as a function of uniaxial strain. In particular, the first four peaks, annotated 1, 2, 3 and 4 in each figure, provide insight into the structure of the 1x1 tunnels associated with the pyrolucite structure, fig S2(c). Peak 1 corresponds to the 'length' of the 1x1 tunnels (lattice parameter c), while Peak 3, corresponds to the 'cross-sectional dimensions' of the 1x1 tunnels (lattice parameters a and b).

Inspection of the RDF traces reveals that the cross-sectional sizes of the 1x1 tunnels change dramatically when stress is imposed upon *bulk* β-MnO_2. In particular, the single peak 3, fig S2(a), at the start of the simulation (unstrained state), shows that the cross-sectional dimensions of the 1x1 tunnels are 4.4x4.4Å. However, under 5% strain, peak 3 broadens and splits into two indicating tunnels with cross-sectional dimensions of 4.2 and 4.5Å and spanning 4.0-4.7Å.

The calculated RDF, fig S2(a), also reveals that the unit lengths of the 1x1 tunnels do not change in bulk MnO_2 under uniaxial strain of 5%; the shape of peak 1 is the same spanning 0 - 5% strain. We note that the microtwinning in the bulk MnO_2, fig 1(a) (main paper), means that the direction of the uniaxial compressive stress imposed aligns with a variety of crystallographic directions. In particular, the [001] direction (along the 1x1 tunnel) will change by 120^o as the crystal reaches a twin boundary (fig 1(a), red oval). Accordingly, compression of the system along, for example, the [001] crystal direction would not align with the [001] of twin domains.

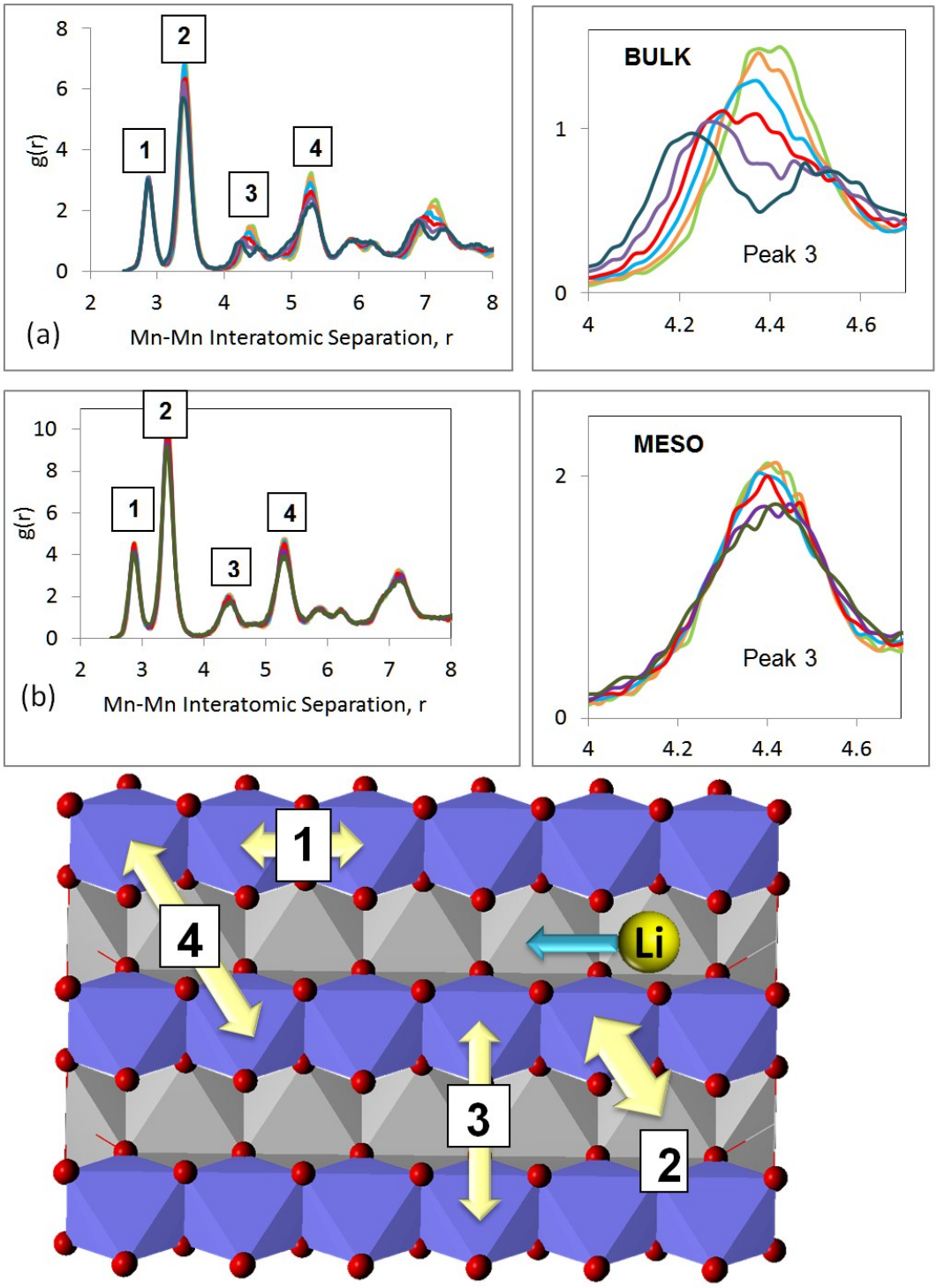

Figure S2 *Mn-Mn Radial Distribution Functions, calculated as a function of strain, for (a) bulk and (b) mesoporous β-MnO_2; Mn-Mn distances are in angstroms. (c) Shows how the first four peaks of the RDF (Peak 1, 2, 3 and 4) correspond to the Mn-Mn distances in the β-MnO_2 crystal structure. Peak 1 corresponds to lattice parameter c, and peak 3 corresponds to the lattice parameter a. Colour notation: strain=0% (light green); strain=1% (orange); strain=2% (blue); strain=3% (red); strain=4% (purple); strain=5% (dark green).*

For the *mesoporous* β-MnO_2, there is almost no change in any of the peaks, fig S2(b), when stress is imposed upon the system. This suggests, surprisingly, that the crystal structure and tunnel dimensions do not change when the material is stressed uniaxially by 5%. To rationalise this behaviour, we measured the volume of the bulk and mesoporous β-MnO_2 under zero strain and 5% strain. The results revealed that under 5% uniaxial strain, the volume of the mesoporous β-MnO_2 reduced by 3.1% and the bulk β-MnO_2 reduced by 2.5%. Presumably, the only way the mesoporous β-MnO_2 could retain its structural integrity is if it expanded into the pore space of the mesoporous β-MnO_2. Indeed, further calculations revealed that the pore volume reduced by 7% at 5% uniaxial strain. Such expansion of the MnO_2 into the pores helps mitigate changes in the crystal structure as a consequence of imposing uniaxial stress. This phenomenon is akin to that of 'Le Chataliers principle' in that the mesoporous β-MnO_2 responds structurally to mitigate the effect of imposed stress.

X-ray Diffraction

The x-ray diffraction patterns, calculated as a function of uniaxial stress, are shown in fig S3(a, b) for the bulk and mesoporous MnO_2 respectively. For the bulk material, several of the peaks split as a function of stress; dotted lines on fig S3 highlight the split peaks and changes to 2θ values. Conversely, for the mesoporous MnO_2, there is no change in the peaks. The complex changes to the XRD are indicative of perturbations to the microstructure and interplanar spacings (1x1 tunnel dimensions).

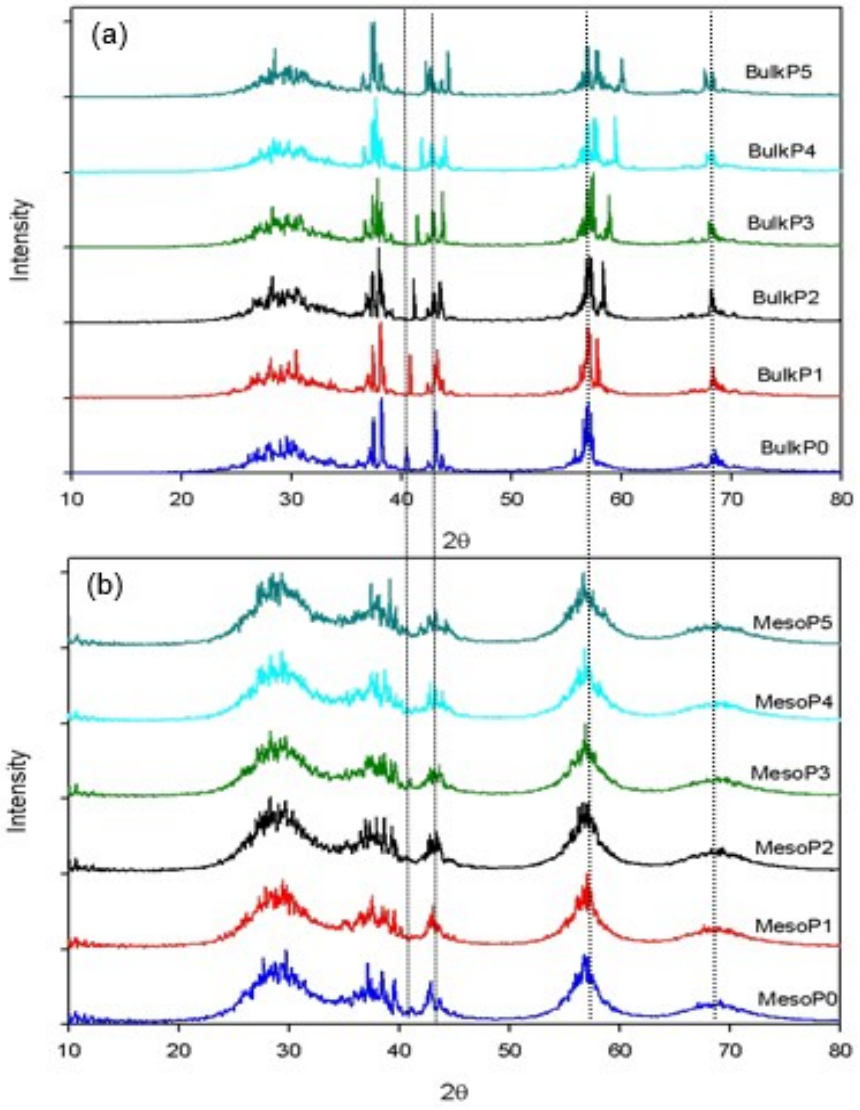

Figure S3 *X-ray patterns for (a) mesoporous β-MnO_2 and (b) bulk β-MnO_2, calculated as a function of strain; P0-P5 indicate strains of 0-5%; the dotted lines on the figure indicate the changes in 2ϑ for the peaks associated with bulk MnO_2 as a function of strain.*

Bulk P0 XRD Indexing

Bulk MnO_2 (P0, unstrained) was indexed as a tetragonal, fig S4, table S1, or orthorhombic, fig S5, table S2, cell.

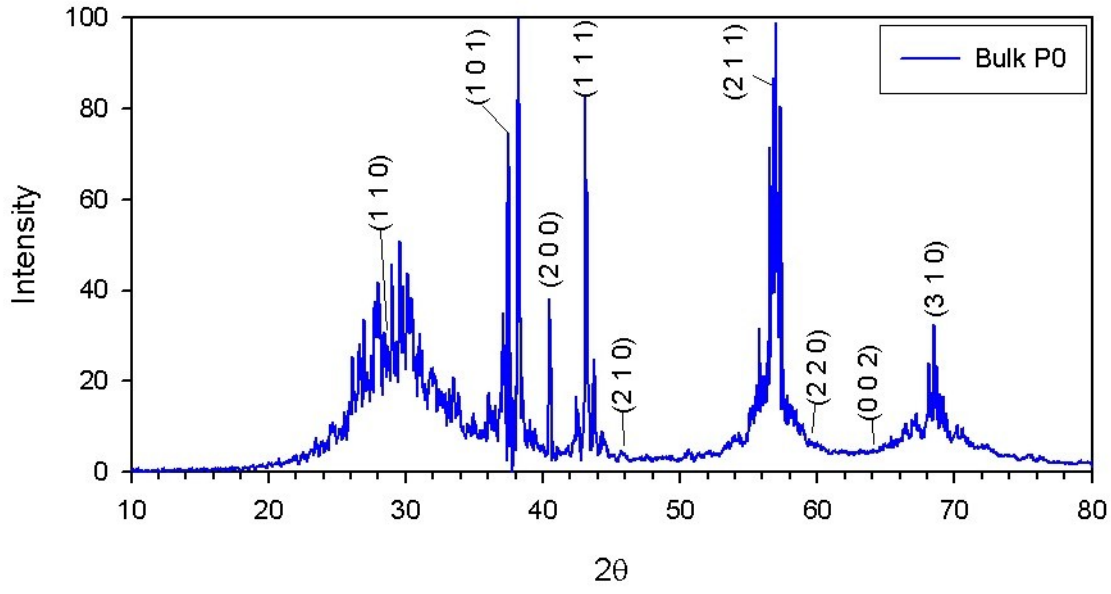

Figure S4 XRD of bulk MnO_2 (P0, unstrained) indexed as tetragonal crystal system.

Table S1 *Observed (2-theta obs.) and expected (2-theta calc.) peak positions for bulk MnO_2 (P0, unstrained), indexed for a tetragonal system.*

h k l	2-theta obs.	2-theta calc.	Difference
1 1 0	28.675	28.659	0.016
1 0 1	37.45	37.249	0.201
2 0 0	40.474	40.976	-0.502
1 1 1	43.103	42.713	0.39
1 1 1	43.226	42.713	0.513
2 1 0	45.711	46.074	-0.363
2 1 1	56.7	56.565	0.135
2 1 1	56.812	56.565	0.247
2 2 0	59.276	59.338	-0.062
2 2 0	59.437	59.338	0.099
0 0 2	64.121	64.592	-0.471

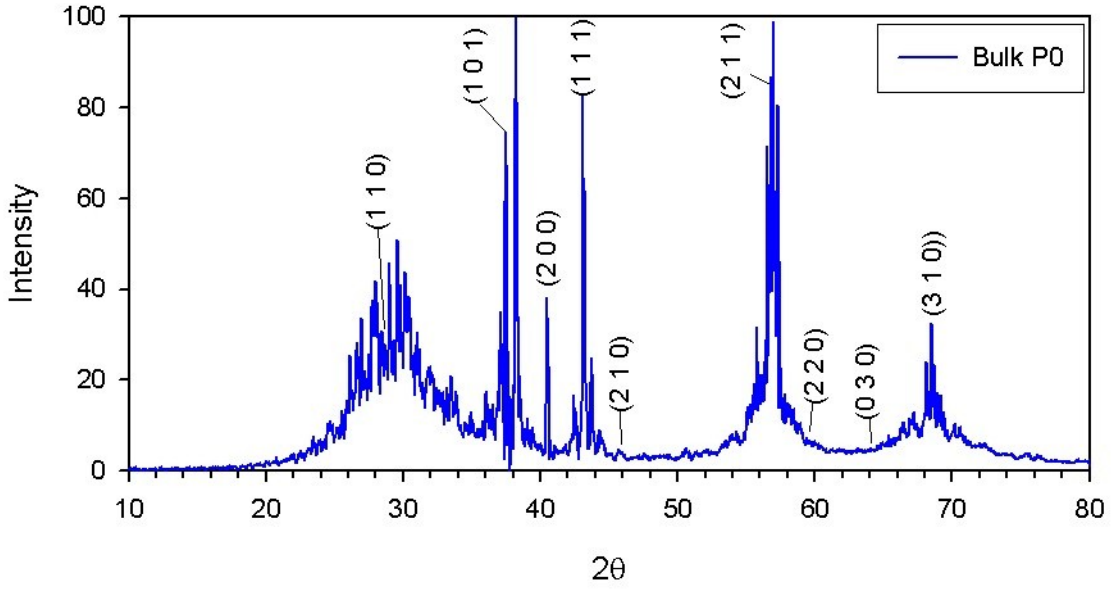

Figure S5 *XRD of bulk MnO_2 (P0, unstrained) indexed as an orthorhombic crystal system.*

Table S2 *Observed (2-theta obs.) and expected (2-theta calc.) peak positions for bulk MnO_2 (P0, unstrained), indexed for an orthorhombic system.*

h k l	2-theta obs.	2-theta calc.	Difference
1 1 0	28.675	28.69	-0.015
1 0 1	37.45	37.641	-0.191
2 0 0	40.474	40.634	-0.16
0 2 0			
1 1 1	43.103	43.168	-0.065
1 1 1	43.226	43.168	0.058
2 1 0	45.711	45.862	-0.151
2 1 1	56.7	56.735	-0.035
2 1 1	56.812	56.735	0.077
2 2 0	59.276	59.409	-0.133
2 2 0	59.437	59.409	0.028
0 3 0	64.121	64.052	0.069
3 1 0			
0 0 2			

3 0 1	72.225	71.964	0.261

Bulk P5 XRD Indexing

Bulk MnO_2 under 5% strain, indexed as a tetragonal system, is shown in fig S6. The corresponding lattice parameters are given in table S3 and show a unit cell volume change of -5.1%.

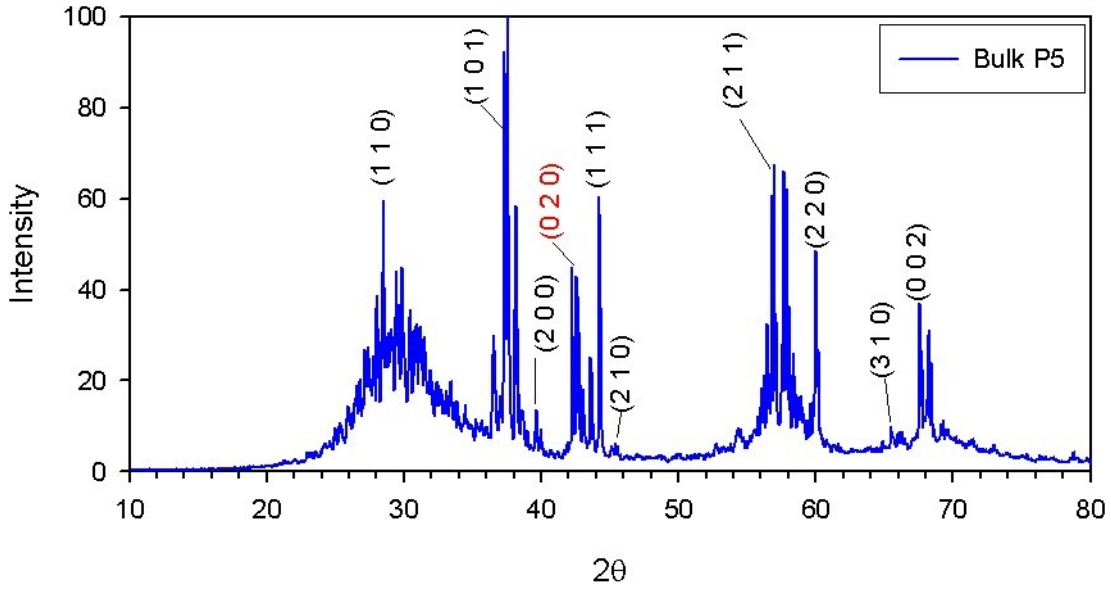

Figure S6 *XRD of bulk MnO_2 (P5, compressed), indexed as a tratragonal crystal system.*

Table S3 *Observed (2-theta obs.) and expected (2-theta calc.) peak positions for bulk MnO_2 (P5, compressed), indexed for a tetragonal system.*

h k l	2-theta obs.	2-theta calc.	Difference
1 1 0	28.675	28.888	-0.213
1 0 1	37.605	38.082	-0.477
2 0 0	39.688	39.783	-0.095
0 2 0	42.58	42.796	-0.216
1 1 1	43.618	43.898	-0.28
1 1 1	44.229	43.898	0.331
2 1 0	45.601	45.419	0.182
2 1 1	56.795	56.844	-0.049
2 1 1	56.978	56.844	0.134
2 2 0	60.026	59.851	0.175
2 2 0			
0 3 0			
3 1 0	65.529	65.638	-0.109
0 0 2	67.667	67.718	-0.051
3 0 1			

The lattice parameters, calculated for bulk MnO_2 (strained, P0, and unstrained, P5) are presented in table S4

Table S4 *Cell parameters for tetragonal MnO2 unit cell.*

	a (Å)	**b (Å)**	**c (Å)**	**V (Å^3)**
Tetragonal bulk P0	4.4015		2.8834	55.8590
Orthorhombic Bulk P0	4.4369	4.3576	2.8328	54.7700
Orthorhombic bulk P5	4.5299	4.2149	2.7679	52.8470
Exp.	4.4008		2.8745	55.6706

Li mobility in mesoporous MnO2

To simulate the mobility of Li within the walls of the mesoporous MnO_2 and their subsequent deintercalation out of the (internal) pore surfaces, Li ions were positioned 'deep' within the walls of the MnO_2, fig S7(a). MD simulation was then used to simulate the diffusion through the host lattice. In particular, MD simulation was performed for up to 2ns at 600, 700, 800, 900, 950, 1000, 1050, 1100 and 1150K, using an NST ensemble (constant Number of ions, constant Stress and constant Temperature). An NST rather than NVE (constant Number of ions, constant Volume and constant Energy) ensemble was used because the framework MnO_2 lattice will likely change its strain state and hence lattice parameter as Li ions are deintercalated from the lattice. NVE would artificially constrain the lattice to constant volume and therefore would not capture the effect of such a structural change. At the end of the simulation, the Li ions are seen to deintercalate, fig S7(b), and decorate the surface of the pore.

Li deintercalation

The surface structure of the (internal) pores of mesoporous MnO_2 will impact upon the Li deintercalation process. Accordingly, the pores were analysed using molecular graphics and revealed that very few 1x1 tunnels lie perpendicular to the pore surface; rather the 1x1 tunnels lie at a variety of different angles to the surface normal, fig S8. Accordingly, the surface 'exit holes' are structurally different and display a wide variety of structural configurations and sizes.

Changes in surface structure during Li deintercallation

After Li deintercalates from the host lattice, the 1x1 tunnels will likely change in structure as they will not have to accommodate the strain associated with Li occupancy. Accordingly, molecular graphics was used to examine the surface of the pores before and after deintercallation, fig S9, S10. Inspection of these figures reveals a remarkable change in structure of the exit sites (circles in fig S9). This can be explained, in part, by realising that as Li resides within the 1x1 tunnel, the tunnel is held in a particular strain state. Upon deintercallation, the 1x1 tunnels can then relax back to their unstrained configuration. Similarly, the coordination of the (deintercallated) Li, on the surface of the internal pore to

the surface oxygen of the MnO_2, also influences the surface structure, fig S10. Such observation also indicates that a polar electrolyte will also exact changes upon the surface structure and hence entrance/exit sites of the host MnO_2.

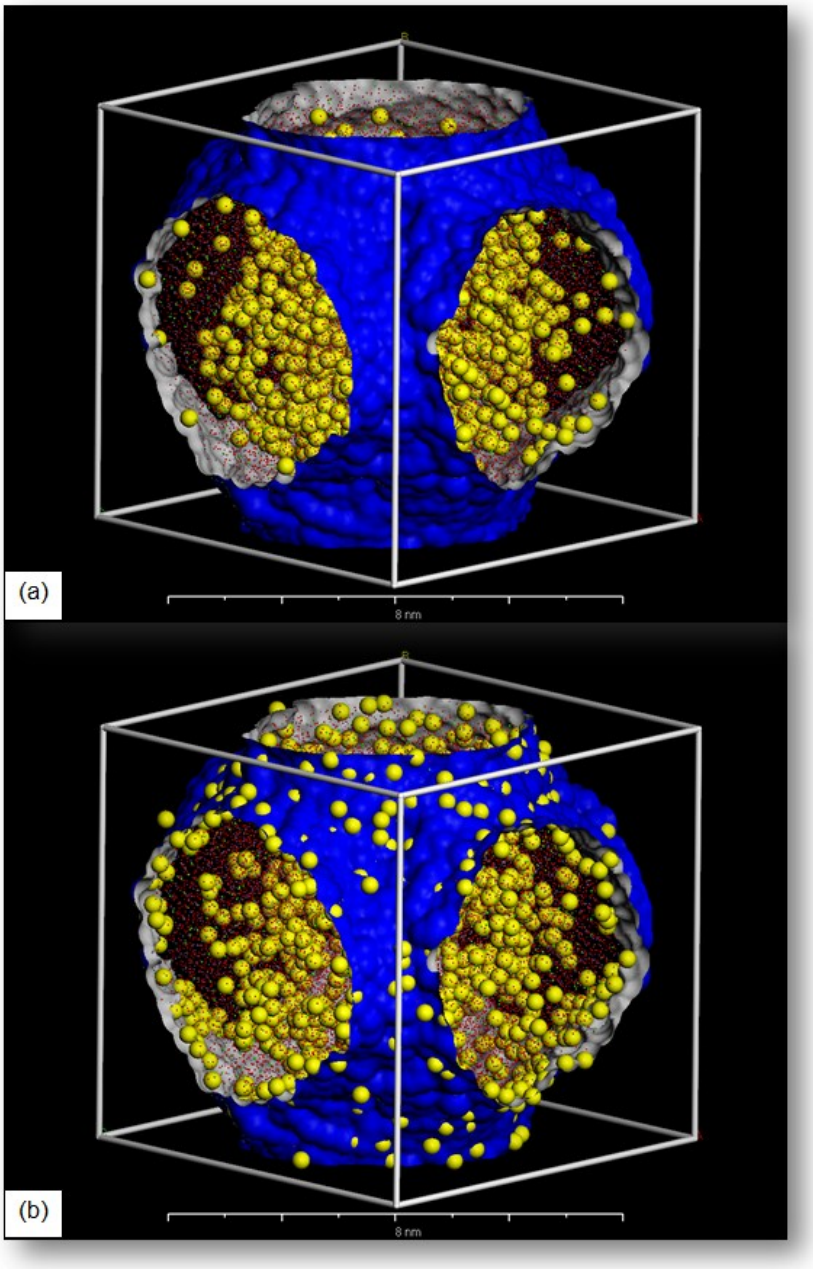

Figure S7 *Li-ions deintercalating from the host MnO_2. (a) Start of the MD simulation showing Li 'deep' within the host lattice. (b) End of the MD simulation showing Li-ions that have migrated to the surface of the pores via the 1x1 tunnels, and deintercalated out of the MnO_2 to reside on the surface of the internal pore of the MnO_2. The surface of the internal pore is coloured blue; Li is coloured yellow.*

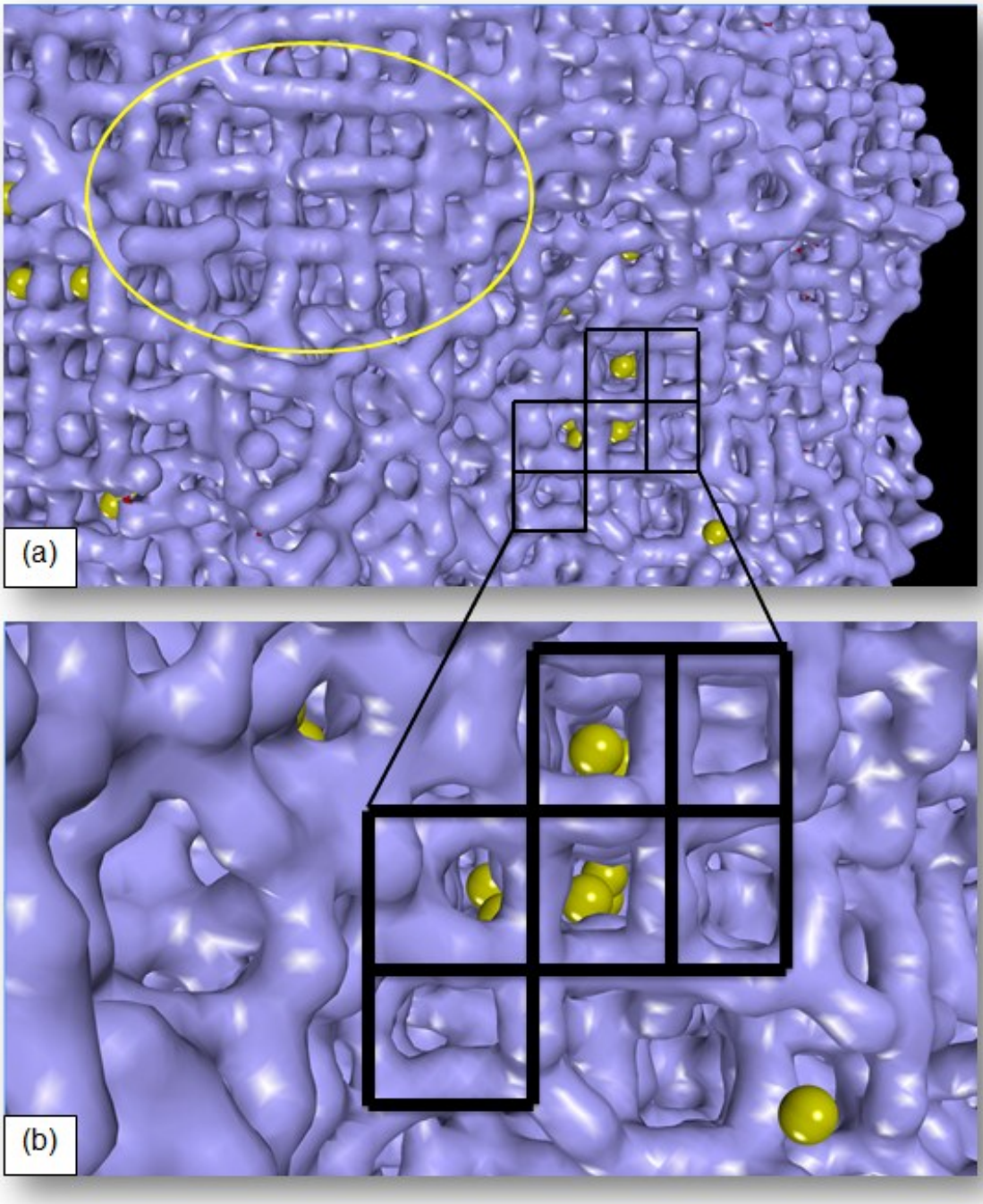

Figure S8 *(a) Surface rendered model of part of the surface of one of the internal pores comprising the mesoporous MnO_2. The image shows a variety of structurally different surface entrance sites. The yellow oval shows a region where an array of 1x1 tunnels lie (close to) perpendicular to the surface of the pore. The six black rectangles also shows 1x1 tunnels in which Li ions, coloured yellow, reside; (b) enlarged segment of (a).*

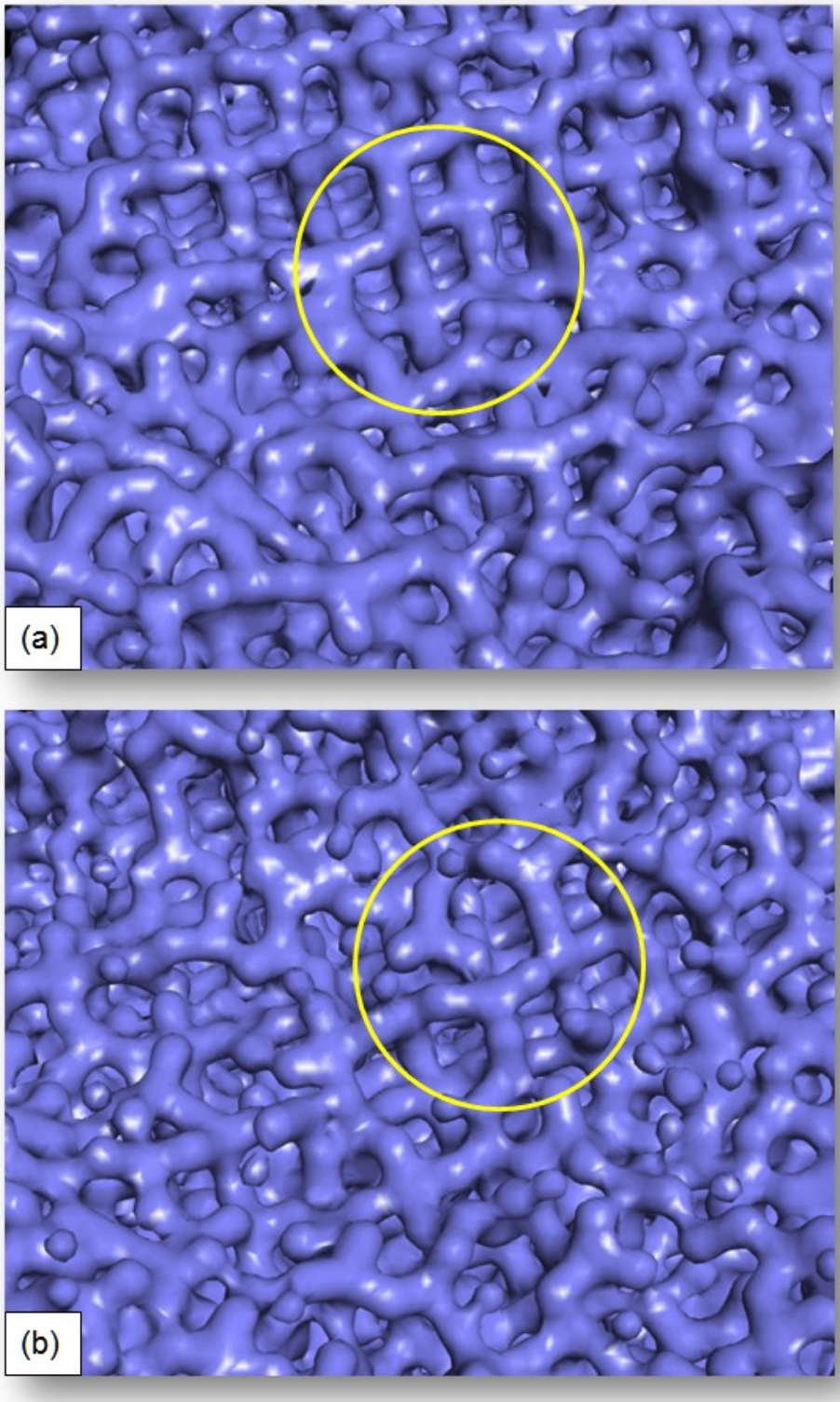

Figure S9 Surface rendered model of the atom positions comprising mesoporous MnO_2 (a) before Li deintercallation, (b) after deintercallation. The figure shows considerable changes in the size and structure of the extrance sites to the 1x1 tunnels. This is more evident if one compares the structure highlighted by the yellow circles.

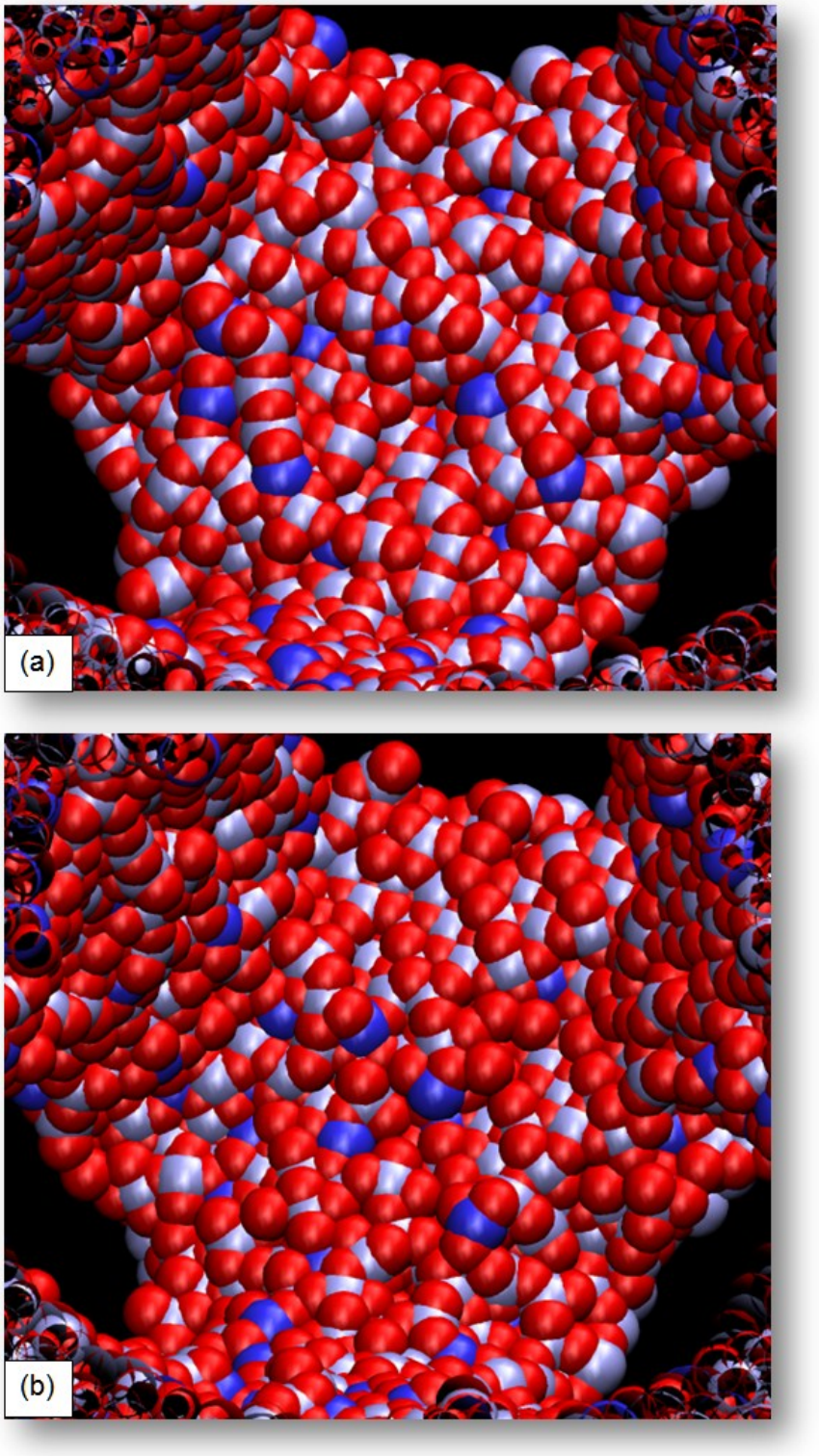

Figure S10 *Snapshots, taken of the MD simulation (a) before Li deintercalation, (b) after deintercallation (Li is not shown) showing the change in surface structure. Specifically, the oxygen ions move out of the surface with respect to the manganese ions to coordinate with the surface lithium. O^{2-} is red, Mn^{4+} is grey and Mn^{3+} is blue.*

Transport Energetics

The activation energy barriers associated with Li-ion mobility and deintercalation can be extracted from the standard Arrhenius equation, using calculated Mean Square Displacements (MSD):

$$MSD = \left\langle r_i^2(t) \right\rangle = \frac{1}{N}\sum_{1}^{N}\left[r_i(t) - r_i(0)\right]^2 = 6D_i t + B \quad (1)$$

$$D_i = A\exp\left(\frac{-E_{act}}{k_B T}\right) \quad (2)$$

$$LnD_i = \frac{-E_{act}}{k_B}\left(\frac{1}{T}\right) + C \quad (3)$$

where D_i is the diffusion coefficient, E_{act} is the activation energy barrier, k_B is the Boltzmann constant, T is the temperature, r_i is the position of ion i and t is time. The activation energy can then be captured from the gradient, $-E_{act}/k_B$, of a graph of natural log of the Diffusion coefficients, calculated as a function of inverse temperature.

We note that the MSD do not change uniformly with time, fig S9; rather the MSD trace comprises large fluctuations in the average velocities of the Li ions. This can be attributed to the variety of processes associated with the Li mobility. These include: the mobility of Li along straight 1x1 tunnels, navigation of Li around twin boundaries and other microstructural defects, the association or binding energy between Li^+ and Mn^{3+} ions, Li arriving at the end of a blocked 1x1 tunnel, deintercalation of the Li from the surface and subsequent diffusion along the (internal) pore surface of the MnO_2. A recent study by Kerisit and co-workers found that the MSD of Li ions within mixed Mn/Ti Oxides show that the MSD is only linear for infinite dilution of Li; the authors attribute such anomalous self-diffusion to Li-Li interactions and association with structural defects.[i]

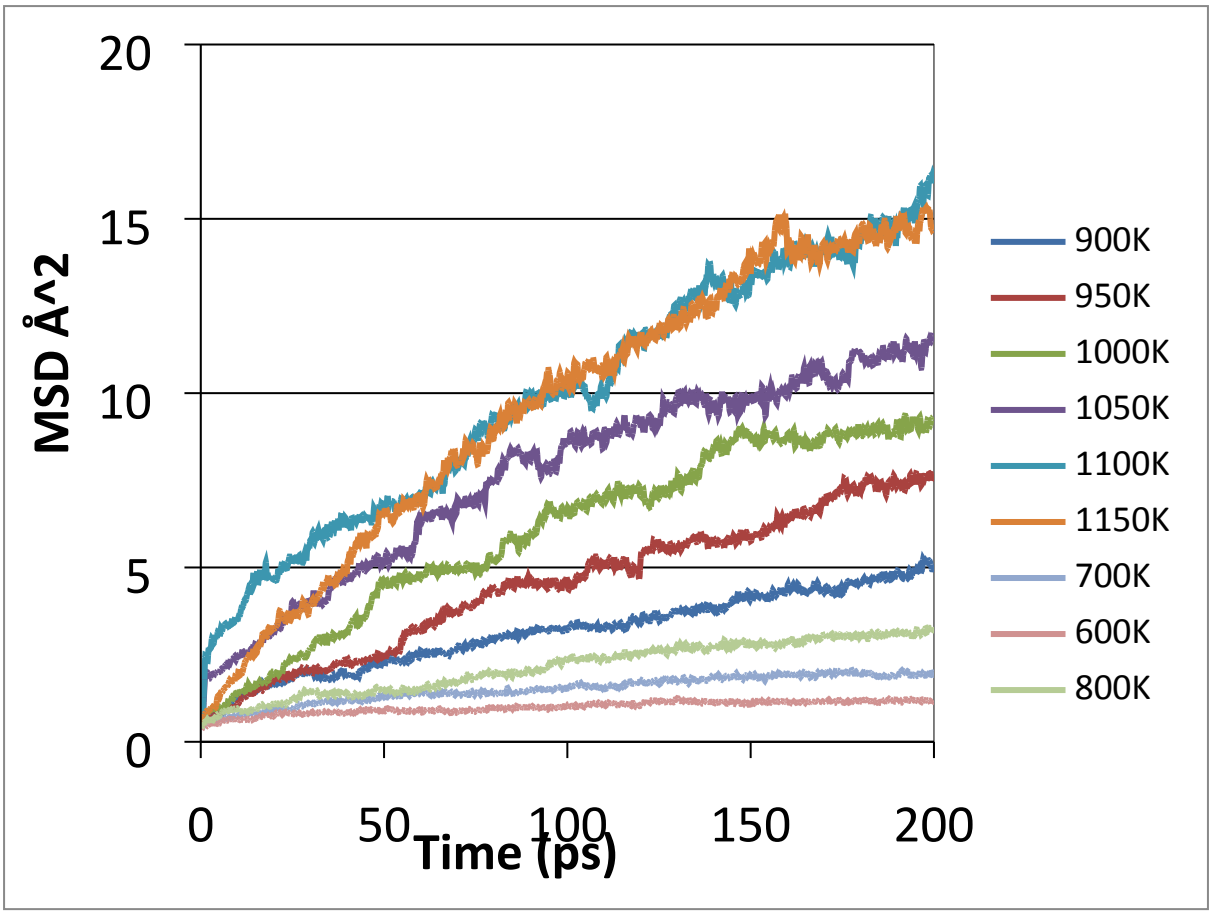

Figure S11 *MSD ($Å^2$) calculated as a function of time (ps) for Li in mesoporous MnO_2. Time up to 200ps is shown; lower temperatures were run for 2ns to reduce statistical noise.*

[i] Kerisit, S.; Chaka, A.M; Droubay, T.C. and Ilton, E.S.
Shell Model for Atomistic Simulation of Lithium Diffusion in Mixed Mn/Ti Oxides
J. Phys. Chem. C, 2014, 118, 24231.